

# A Class of Haar Functions on Unit Disk

Chen Wei, Li Jian, and Qi Dongxu

Faculty of Information Technology, Macau University of Science and Technology, Macau

Email: jlxy2004@163.com, linxli3@yahoo.com, dxqi@must.edu.mo

**Abstract**—In order to investigate the effective circular image analysis method, a class of Haar functions defined on the unit disk, named as disk Haar Functions (DHF), is introduced in this paper. Compared with traditional bivariate tensor product orthogonal functions (TPOFs), DHFs have great advantages in handling the circular images. Experimental results demonstrate that DHFs is more suitable for representing images on circular region than TPOFs.

**Index Terms**—circular image, haar functions, orthogonal

## I. INTRODUCTION

Spectral analysis method based on orthogonal functions has been successfully used in signal processing. The common way for representing two-dimension (2D) signals such as digital image is tensor product orthogonal functions(TPOFs)[1]. In this paper, circular images are referred to such a class of images whose effective region is circular area. There are lots of circular images in practical applications, such as interference patterns in optical physics, impact crater images on celestial surface and many trademark logos. Before these circular images are applied to orthogonal transforms using 2D TPOFs, they have to be extended to rectangular region by means of regional extrapolation [2]-[4]. The edge error called edge effect will be occurred in reconstruction images. Fig.1 shows the results that a binary image was represented by FFT. It can be seen that there are obvious edge effects in reconstructed images.

Haar functions is a class of complete orthogonal functions set in  $L^2[0,1]$ , which take values of 1,-1 and 0 if the standardization coefficients are not taken into consideration. As a typical complete discontinuity orthogonal functions set, Haar functions have the important theory significance and practical application value[5].

In order to efficiently represent the circular images, a class of orthogonal Haar functions on the unit disk, named as disk Haar functions (DHF) were constructed in this paper. The definition domain of DHFs is the unit disk denoted as  $D=\{(\rho, \theta), 0 \leq \rho \leq 1, 0 \leq \theta \leq 2\pi\}$ . By an equal-area partition on  $D$ , a one-to-one mapping relationship between  $D$  and the 2D tensor product Haar functions(TPHFs) is established and then DHFs could be obtained directly.

The organization of this paper is as follows. Section 2 briefly reviews the singer variable and 2D tensor product Haar functions; Section 3 presents the derivation of the DHFs; Section 4 presents the algorithms of decomposition and reconstruction for circular images under DHFs, i.e. DHFs transform; Section 5 demonstrates the effectiveness of DHFs by two typical examples, and section 6 provides the conclusions and future works.

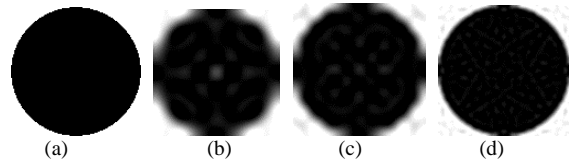


Figure 1. Original image(a) and Reconstructed images by FFT with number of coefficients of 50,100 and 500, respectively (b~d).

## II. DISK HAAR FUNCTIONS

### A. Traditional Haar Functions

Haar functions were introduced in 1910 by A.Haar[6], denoted as  $\{h_i(x)|i=0,1,2,\dots,0 \leq x \leq 1\}$ . The first 16 Haar functions are displayed in Fig. 2.

Bivariate tensor product Haar functions (TPHF) on planar domain (denoted as  $S=\{(x,y), 0 \leq x,y \leq 1\}$ ) are defined as  $H_{ij}(x,y)=h_i(x)h_j(y), i=1,2,\dots,2^m, j=1,2,\dots,2^n$ . The first 64 TPHFs are displayed in Fig. 3.

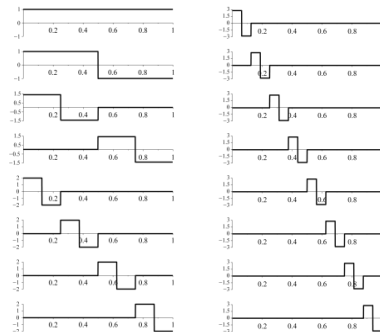


Figure 2. Haar functions(1D)

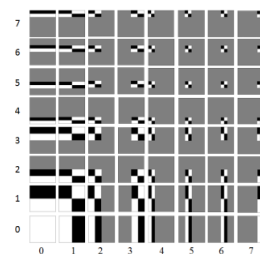


Figure 3. Haar functions(2D)

B. Disk Haar Functions(DHFs)

1) Equal-area partition on unit disk

Haar functions are piecewise constant which take values of 1,-1 and 0 if the standardization coefficients are not taken into consideration. Through the equal-area partition on  $D$  ( $D=\{(\rho,\theta),0\leq\rho\leq 1,0\leq\theta\leq 2\pi\}$ ), a one-to-one mapping relationship between  $D$  and 2D TPHFs is established and the DHFs could be obtained directly.

We will use the following rules to divide the unit disk [7]:

- The unit disk is uniformly divided along the radial direction  $\rho$  into  $U$  sections, with the separating circles located at  $\{u/U, u=1,2,\dots,U\}$ , and  $U$  is set  $2^L, L=0,1,2,\dots$ .
- The  $u$ th ring-shape section is equally divided into  $4(2u-1)$  sectors by radii starting from the origin.

It can be shown that the unit disk  $D$  is divided into  $4U^2$  sub-regions denoted as  $\{\Omega_{uv}|u=1,2,\dots,U,v=1,2,\dots,4(2u-1)\}$ , each of which has an area of  $\pi/4U^2$ . The partition result when  $U=8$  is illustrated in Fig. 4.

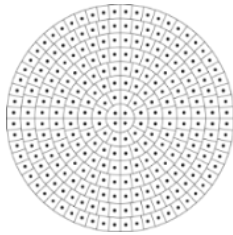


Figure 4. Equal-area partition on unit disk

2) Disk haar functions (DHFs)

After the equal-area partition on  $D$  in accordance with the above rules,  $4U^2$  sub-regions are generated. Discrete 2D TPHFs are denoted as  $\{H_{ij}(x,y)|x=1,2,\dots,2^m;y=1,2,\dots,2^n\}$ . When  $2^m=2^n=2U$ , i.e,  $m=n=\log_2 U+1$ , the planar domain  $S$  is also divided into  $2U \times 2U$  square sub-regions. We could establish a one-to-one mapping relationship between sub-regions in  $D$  and  $S$ . DHFs are denoted as  $DH_{ij}(u,v)|u=1,2,\dots,U;v=1,2,\dots,4(2u-1)$ . The pseudo code that mapping  $H_{ij}(x,y)$  to  $DH_{ij}(u,v)$  is as follows.

```

input : Hij(x,y)
output : DHij(u,v)
for u = 1 : U
    v = 1 ;
    for k = 1 : u
        DHij(u,v) =  $\frac{2}{\sqrt{\pi}}$  Hij(U-k+1,U+u) ;
        v = v + 1 ;
    end
    for k = 1 : 2u - 1
        DHij(u,v) =  $\frac{2}{\sqrt{\pi}}$  Hij(U-u+1,U+u-k) ;
        v = v + 1 ;
    end
    for k = 1 : 2u - 1
        DHij(u,v) =  $\frac{2}{\sqrt{\pi}}$  Hij(U-u+k+1,U-u+1) ;
        v = v + 1 ;
    end
end
    
```

```

DHij(u,v) =  $\frac{2}{\sqrt{\pi}}$  Hij(U+u,U-u+k+1) ;
v = v + 1 ;
end
for k = 1 : u - 1
    DHij(u,v) =  $\frac{2}{\sqrt{\pi}}$  Hij(U+u-k,U-u) ;
    v = v + 1 ;
end
end
    
```

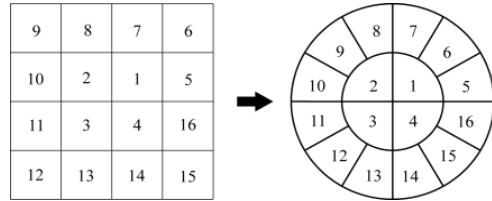


Figure 5. Mapping

Fig. 5 shows the one-to-one mapping relationship between  $H_{ij}(x,y)$  and  $DH_{ij}(u,v)$  when  $U=2$ . The first 64 DHFs are displayed in Fig. 6.

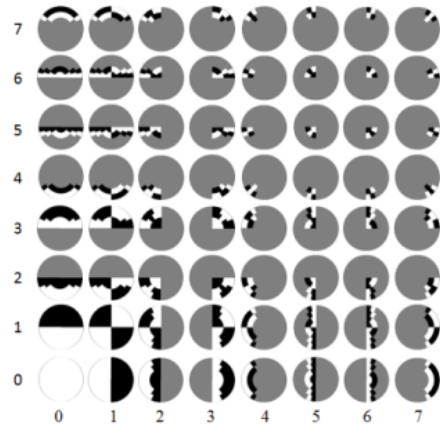


Figure 6. The first 64 DHFs

The set of  $\{DH_{ij}(u,v)\}$  is orthogonal over  $D$  :

$$\langle DH_{ij}(u,v), DH_{pq}(u,v) \rangle = \delta_{ipjq}$$

where  $\delta$  is the Kronecker symbol, i.e.  $\delta_{ipjq}=1$  if  $i=p \wedge j=q$  and 0 otherwise.

III. DHF TRANSFORM

A. Preprocessing

We have seen in previous sections that the structure of DHFs consists of a certain polar sectors. However, a digital image is usually defined by a set of square Cartesian pixels. It can be easily verified that the locations of the polar pixels do not coincide with those of Cartesian pixels. Therefore, we have to derive the polar counterpart of a given Cartesian image. This issue can be resolved by applying an image interpolation procedure. In our simulation studies the image value at a polar pixel is calculated based on bicubic interpolation which has the third order accuracy. With this pattern of polar pixels, image is expressed as  $\{f(u,v), u=1,2,\dots,U; v=1,2,\dots,4(2u-1)\}$ .

B. Image Representation by DHFs

After preprocessing, the image  $f(u,v)$  which is defined on unit disk has the following representation in terms of DHFs

$$\tilde{f}(u,v) = \sum_i \sum_j C_{ij} \cdot DH_{ij}(u,v)$$

where the coefficients  $C_{ij}$  are given by

$$C_{ij} = \sum_{u=1}^U \sum_{v=1}^{4(2u-1)} f(u,v) \cdot DH_{ij}(u,v)$$

IV. APPLICATION EXAMPLES

A. Interference Pattern Reconstruction

Interference pattern is the output from interferometer, and interference fringes are the traces of points which have the same optical path difference. The processing and analysis for interference pattern is directly related to the parameters we want to measure. The effective region of interference pattern is usually circular. A considerable error near the edge called edge effect in reconstruction result will be introduced by traditional 2D tensor product orthogonal functions.

This section presents an actual interference data and results used to validate the theoretical framework presented above, and we establish the feature representation capability of DHFs through image reconstruction. A comparative analysis between DHFs and FFT is given.

An optical interference image in Fig. 6(a) is used, which is expressed as  $\{f(u,v), u=1,2,\dots,U; v=1,2,\dots,4(2u-1)\}$  after preprocessing. Fig. 7 (b)~(e) show the reconstructed results by DHFs with different numbers of coefficients. With the same numbers, reconstructed results by FFT are shown in Fig. 7(f)~(i). Comparing these corresponding images, we can conclude that by DHFs, the quality of reconstructed images are much better than those by using usual tensor product functions for disk images.

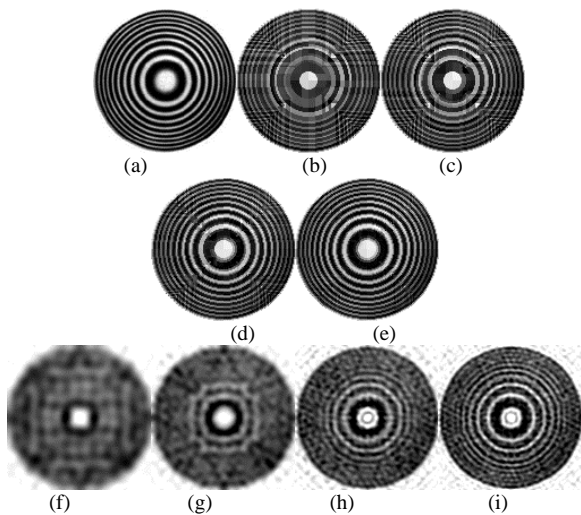


Figure 7. (a) Original optical interference image. (b)~(e) Image reconstruction from DHFs up to items of 100, 200, 500 and 1000, respectively. (f) ~ (i) Image reconstruction from FFT up to same items with DHFs, respectively.

To compare more objectively the performances of the two approaches in terms of image reconstruction, we have experimented on more different numbers of decomposing coefficients for image recovery. Specifically, coefficients up to  $\{i,i=1..8000\}$  were used to reconstruct the image respectively. The quality of each reconstructed image is measured in terms of peak signal-to-noise ratio (PSNR). The test results are shown in Fig.8, from which an important conclusion can be drawn that DHFs has better performance than FFT in circular image representation.

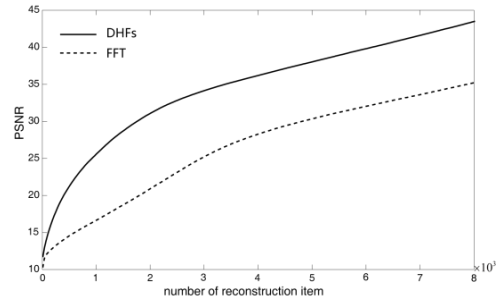


Figure 8. Quality of reconstructed images

B. Spectrum Analyses of Lunar Craters

Celestial craters are greatly small bunches of ring pit structures on the surface of moon, Mars and other planets. They are the most significant features on the surface of planets and are of the windows to study the planets internal material. Study on the craters can provide a large amount of information for celestial status, evolutionary history, cratering mechanism and knock-on effect. For example, the relative age and surface characteristics of the planets could be inferred through the scale frequency distribution and space statistical data of craters. The study of crater morphology could promote the researches of celestial geomorphology such as natural erosion process, regional difference of geological material and distribution of sub-surface volatile matter[8]-[10].

As most of craters are circular, it is suitable for craters analysis by DHFs. 10 typical CCD images of lunar craters captured by Chang'e-1 are selected shown in Fig. 9.

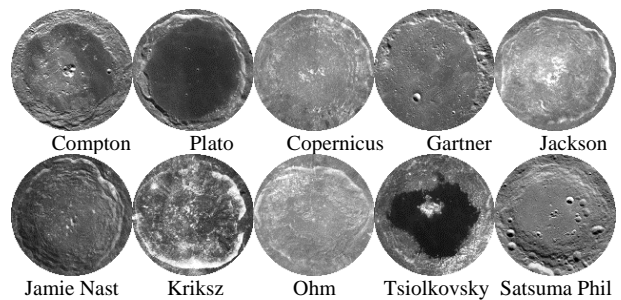


Figure 9. 10 CCD images of lunar craters from Chang'e-1

These crater images were represented by DHFs, and the energy of each crater could be calculated by the formula of  $E = \sum_{i=1}^n \|c_i\|^2$ , where  $c_i$  denotes the decomposition coefficient and  $n$  remarks the number of coefficients.

Energy of each crater as a function of  $n$  from 1 to 8000 is shown in Fig.10, from which two conclusions can be drawn. Firstly, for small numbers, approximately  $n < 500$ , the energy of each crater increases significantly. After this point, all crater energies tend to be stable respectively. Secondly, each crater has its different energy. As a kind of feature, energy can reflect the differences among craters. It is helpful to classify and recognize the craters which are very useful in crater analysis. Fig. 11 illustrates the energy of each crater when  $n=500$ .

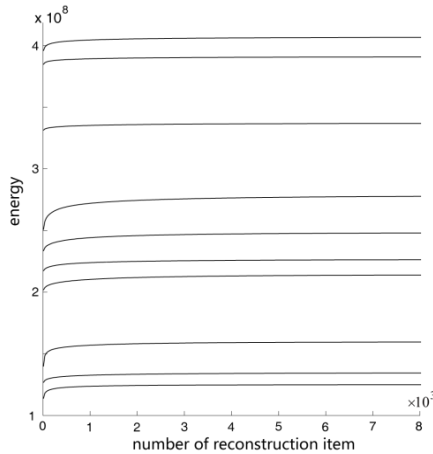


Figure 10. Energy of each crater

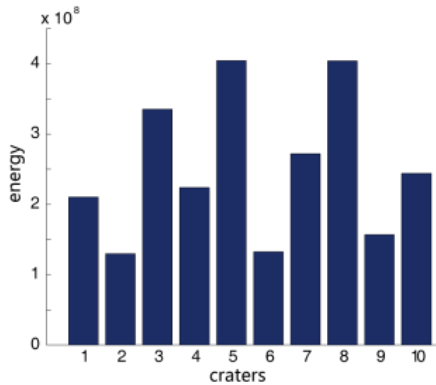


Figure 11. Energy of craters ( $n=500$ )

## V. CONCLUSION AND REMARKS

We construct a class of Haar functions defined on the unit disk named as DHFs. It is obtained through the equal-area partition on unit disk and mapping to the mesh of 2D tensor product Haar functions. The construction method is simple and intuitive, and the computing complexity of decomposition and reconstruction are

lower. The results of examples show that DHFs has more advantages over traditional TPOFs for circular image representation. The program for processing data in this paper provides the base in classification and recognition of lunar craters. In the following works, we will investigate and study the applications of DHFs in lunar craters analysis, especially the relationship between frequency spectrum and geological attributes such as ages of craters.

## ACKNOWLEDGEMENTS

This work was supported by the National Basic Research Program of China under Grant 2011CB302400, and the Science and Technology development Fund of Macau under Grant 006/2011/A1.

## REFERENCES

- [1] R. C. Gonzalez and R. E. Woods, "Digital image processing. upper saddle river," NJ: Prentice Hall, 2002.
- [2] D. J. Bone, H. A. Bachor, and R. J. Sandeman, "Fringe-pattern analysis using a 2-D Fourier transform," *Applied Optics*, vol. 25, pp. 1653-1660, 1986.
- [3] C. Roddier and F. Roddier, "Interferogram analysis using Fourier transform techniques," *Applied Optics*, vol. 26, pp. 1668-1673, 1987.
- [4] J. J. Talamonti, R. B. Kay, and D. J. Krebs, "Numerical model estimating the capabilities and limitations of the fast fourier transform technique in absolute interferometry," *Applied Optics*, vol. 35, pp. 2182-2191, 1996.
- [5] Q. D. X, S. R. X, and L. J, *Discontinuous Orthogonal Functions*, Beijing, China: Science Press, 2011.
- [6] A. Haar, "Zur theorie der orthogonalen funktionensysteme," *Mathematische Annalen*, vol. 69, pp. 331-371, 1910.
- [7] Y. Xin, M. Pawlak, and S. Liao, "Accurate computation of Zernike moments in polar coordinates," *Image Processing, IEEE Transactions*, vol. 16, pp. 581-587, 2007.
- [8] N. G. Barlow and C. B. Perez, "Martian impact crater ejecta morphologies as indicators of the distribution of subsurface volatiles," *Journal of Geophysical Research*, vol. 108, pp. 5085, 2003.
- [9] B. D. Bue and T. F. Stepinski, "Machine detection of Martian impact craters from digital topography data," *Geoscience and Remote Sensing, IEEE Transactions*, vol. 45, pp. 265-274, 2007.
- [10] L. X. Y, L. J. J, M. L. L, and L. C. L, "A review of impact-crater detection," *Astronomical Research & Technolgy*, vol. 9, pp. 203-212, 2012.

**Chen Wei** was born in 1986, Ph.D. candidate. His research interests include computer aided geometric design and image processing.

**Li Jian** was born in 1975, Ph.D. candidate. His research interests include computer graphics and

**Qi Dongxu** was born in 1940, professor, Ph.D. supervisor. His research interests include numerical analysis and computer graphics.